Author ORCID: https://orcid.org/0009-0009-6367-4655

Corresponding author: O. L. Konovalov <konovalovol@bsu.by>

Date: July 30, 2026

Model and algorithm for constructing a horizon surface in the vicinity of a single fault

O. L. Konovalov [1*]

[1]Belarusian State University, Minsk, Belarus

July 30, 2026

Abstract

The article addresses the problem of constructing 3D structural models of geological horizons under faulting conditions. The most labor-intensive stage of structural reservoir modeling is the construction of horizon surfaces that must simultaneously fit seismic data and satisfy structural consistency conditions near faults. It is proposed to reduce the problem of recovering the "unreliable" portion of the horizon surface to solving a mixed boundary value problem with a free boundary (BVPFB) in a variational formulation. The sought surface is defined as a minimizer of an energy functional representing a weighted combination of the Dirichlet energy and the area functional. The weight parameter θ allows the geologist to tune the balance between smoothness and realism of the surface shape near the fault. An original edge-based discretization is developed, yielding a linear problem for any value of θ. Algorithms for constructing the initial triangulation with topological cutting and for the consistent movement of the free boundary are proposed. A practical approach to handling self-intersection of the cut edges is described, naturally extending the algorithm to the case of reverse faults. Results of model tests and testing on real geological objects are presented.

Keywords: structural model, horizon surface, tectonic fault, boundary value problem with free boundary, energy functional, triangulation, combinatorial topology, sparse LU factorization.

1 Introduction

Construction of a three-dimensional structural model of a deposit is a fundamental stage of geological modeling. The key and most labor-intensive element of this process is the modeling of horizon surfaces — geological boundaries of strata that fix stratigraphic marks. The constructed surface must, on the one hand, maximally conform to observational data (seismic survey, wells) and, on the other hand, satisfy the conditions of structural modeling: the condition of realism of the horizon surface shape in the vicinity of tectonic faults and the topological conditions of relationships between structural surfaces.

*konovalovol@bsu.by

When forming a structural model, a primary horizon surface is first constructed, maximally conforming to seismic data. However, in areas adjacent to faults, due to the heterogeneity of acoustic properties of the rock mass in the vicinity of the disruption, such a surface is unreliable. Consequently, the need arises to recover this portion of the surface. Hereinafter, we refer to it as the modeled (unreliable) part of the surface, and the remaining part as the reliable part.

Existing approaches to structural modeling in the vicinity of faults can be divided into two groups. The first group — implicit methods (implicit surface modeling), in which the surface is defined as a level set of a scalar field determined by interpolation [1, 2, 18, 19]. These methods are robust but do not ensure exact topological consistency with fault surfaces: the intersection of the horizon with the fault is determined a posteriori, which can lead to geometric contradictions [22, 24]. The second group — explicit methods (explicit surface modeling), in which the surface is constructed directly in the form of a triangulation. These include methods based on DSI (Discrete Smooth Interpolation) [3] and GRP (Gradual Deformation) [4]. Explicit methods provide direct control of topology; however, the construction of cuts along faults within these methods is generally performed heuristically, without reduction to a mathematically correct boundary value problem.

A review of the current state of the field shows that, despite significant progress in the development of both implicit and explicit structural modeling methods [20, 21, 22, 23, 24], the problem of formally reducing the task of recovering a horizon surface in the vicinity of a fault to a boundary value problem with a free boundary remains open. Existing approaches either avoid explicit specification of the cut (implicit methods) or use heuristic procedures for its construction (explicit methods). In this work, an approach is proposed in which the problem of recovering the unreliable part of the horizon surface is formulated as a mixed boundary value problem with a free boundary (BVPFB) in a variational formulation.

The main results of this work are as follows. The problem of recovering a horizon surface in the vicinity of a single tectonic fault is reduced to a mixed boundary value problem with a free boundary in a variational formulation, in which the sought surface is defined as a minimizer of an energy functional. A weighted combination of the Dirichlet energy and the area functional, controlled by a parameter θ, is proposed, allowing the geologist to tune the balance between smoothness and realism of the surface shape near the fault. An original linear edge-based discretization of the area functional is developed, by virtue of which the minimization problem reduces to solving a single system of linear algebraic equations for any value of θ — despite the nonlinearity of the continuous Euler–Lagrange equation for $\theta < 1$. An algorithm for constructing the initial triangulation with topological cutting and an algorithm for consistent movement of the free boundary, ensuring continuity of boundary conditions, are proposed. A practical approach to handling self-intersection of cut edges is described, naturally extending the algorithm to the case of reverse faults. Results of model tests and testing on real geological objects are presented.

2 Formalization of the modeling problem

2.1 Choice of surface representation

Before proceeding to the formal problem statement, it is necessary to determine the method of surface representation. For this purpose, we analyze the main types of discontinuity of geological strata.

There are two main types of disruption — normal faults and thrusts, corresponding to normal and reverse types of single faults (Fig. 1). The real picture of tectonic disruption can be more complex: both types can be combined within a single fault. However, to understand the essence of the proposed approach, we limit ourselves to considering these two cases.

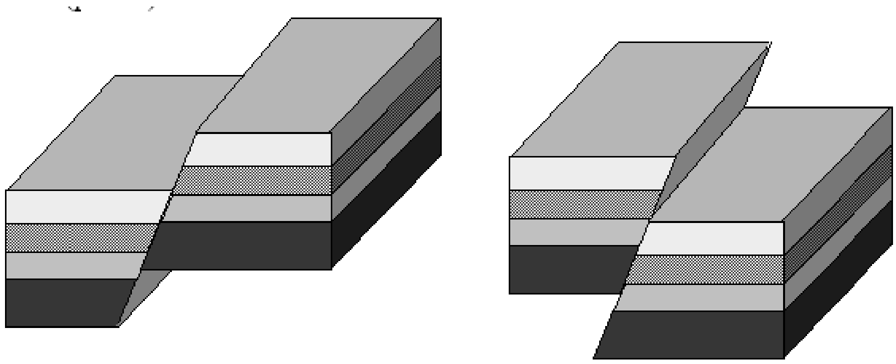

Figure 1: Normal (left) and reverse (right) faults. In a normal fault, the horizon surface is uniquely projected onto the horizontal plane; in a reverse fault, the edges overlie each other.

The fundamental difference is as follows. In the case of a *normal fault*, the horizon surface can be uniquely (bijectively) projected onto the horizontal plane, i.e., represented as a function defined on some subset of $\mathbb{R}^2$. For a *reverse fault*, the horizon surface cannot be uniquely projected onto the horizontal plane, since the edges of the horizon overlie each other. In this case, the surface does not admit a non-parametric (functional) representation and must be specified as a more general geometric construction — as a two-dimensional manifold with boundary.

The representation of the modeled surface in non-parametric (functional) form is preferable, since it allows formulating the modeling problem in a simpler form and obtaining a more robust algorithm for practical problems. In this article, we limit ourselves to the case of a normal fault; generalization to reverse faults and fault networks will be considered in a separate publication.

2.2 Formal statement of the boundary value problem for a normal fault

Consider the representation of the surface in non-parametric (functional) form. The modeled surface will be sought in the class of functions $u : \Omega \to \mathbb{R}$, where the domain Ω (unreliability domain) is some bounded closed subset of $\mathbb{R}^2$.

Realism condition

In the unreliability domain, there is no reliable information about the internal structure of the surface. The only data are the boundary conditions on Γ_0 and Γ. Among the infinite set of surfaces satisfying these conditions, it is necessary to choose the most "natural" one — not containing unphysical oscillations and not deviating without reason from the trend of the reliable part.

A natural way to formalize this requirement is the *variational principle*: the sought surface must minimize some energy functional $E(u)$ characterizing the degree of "deformation" of the surface relative to the plane. Such a principle is natural in the absence of data on the internal structure of the domain: among all surfaces with given boundaries, the least deformed one is selected.

The specific choice of the functional $E(u)$ and its connection with existing interpolation methods used in geological modeling are discussed in Section 3.2.1. Here we note that minimizing the Dirichlet energy $E(u) = \int_\Omega |\nabla u|^2 \, dx \, dy$ leads to the Laplace equation (a linear problem), while minimizing the area functional $E(u) = \int_\Omega \sqrt{1 + |\nabla u|^2} \, dx \, dy$ leads to the minimal surface equation (a nonlinear problem). In this work, a weighted combination of these two functionals is used.

Boundary conditions

The reliable part of the horizon surface, by construction, maximally conforms to observational data. For the modeled surface to possess the same property, it must be a *smooth continuation* of the reliable part. Since the only reliable information in the unreliability domain is the boundary of contact between the reliable and modeled parts, it is reasonable to require not only continuity along this boundary but also smoothness along it.

Let Γ_0 be the outer contour of the unreliability domain Ω, h be the specified depth, and g be the value of the normal derivative of the reliable part of the horizon surface on Γ_0. Then:

$$u = h \quad \text{on } \Gamma_0, \tag{1}$$

$$\frac{\partial u}{\partial n} = g \quad \text{on } \Gamma_0. \tag{2}$$

Topological consistency condition with the fault

Assume that the fault surface also has a non-parametric representation: $w : \Omega_w \to \mathbb{R}$, where Ω_w is a bounded, closed, and convex subset of $\mathbb{R}^2$ belonging to Ω.

The topological requirement for the structural model informally consists in the following: the fault surface forms a "cut" on the sought surface. Formally, this means that inside the contour Γ_0 there is an inner contour Γ, which is the projection of the cut edge onto the xy plane. The boundary of the domain Ω consists of two contours: the outer Γ_0 and the inner Γ. The inner contour Γ consists of two smooth non-intersecting curves γ_1 and γ_2 (cut edges) forming the left and right edges of the cut (Fig. 2). The contour Γ belongs to the domain Ω_w, and the ends of the cut edges (cut vertices) A and B belong to the boundary of Ω_w.

The topological condition is formally written as a boundary condition of the first kind:

$$u = w \quad \text{on } \Gamma. \tag{3}$$

Final statement of the boundary value problem for a normal fault

Let $\Omega \subset \mathbb{R}^2$ be a bounded domain whose boundary consists of two simple (non-self-intersecting) contours Γ_0 and Γ, i.e., Ω is a doubly connected domain with a "hole." The

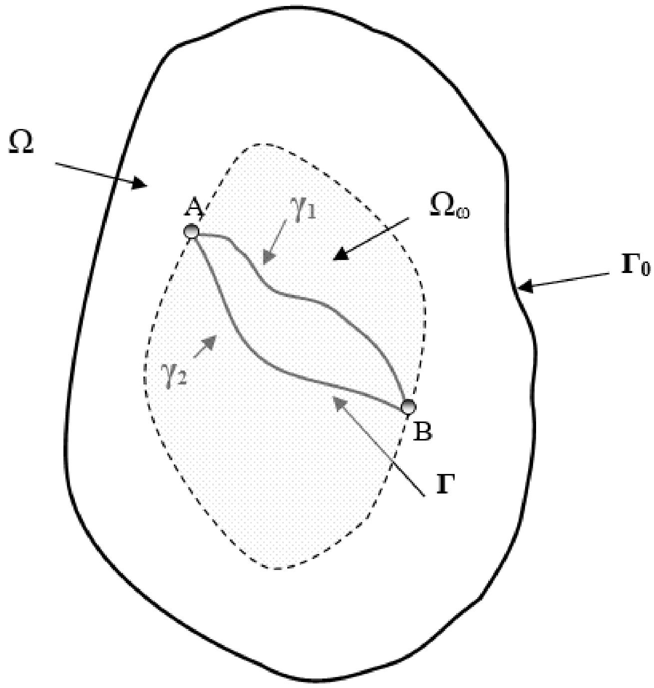

Figure 2: Ω — domain of the horizon surface with a cut; Γ_0 — outer boundary of Ω (contour of the unreliability domain); Γ — inner boundary of Ω (cut contour) consisting of curves γ_1 and γ_2; Ω_w — domain of the fault surface function w; A and B — cut vertices belonging to the boundary of Ω_w.

problem consists in finding the free part of the boundary Γ and the function u satisfying the constraints:

$$E(u) \to \min \quad \text{in } \Omega, \tag{4}$$

$$u = h \quad \text{on } \Gamma_0, \tag{5}$$

$$\frac{\partial u}{\partial n} = g \quad \text{on } \Gamma_0, \tag{6}$$

$$u = w \quad \text{on } \Gamma. \tag{7}$$

Here $E(u)$ is the energy functional, whose specific form is determined in Section 3.2.1; the functions h and g, specified on the outer boundary of the unreliability domain, ensure smooth conjugation of the recovered surface with the unchanged part of the horizon; the function w specifies the fault surface.

It is required that the sought free boundary Γ be a closed contour belonging to the domain of the fault function Ω_w, and consist of two smooth, open, non-intersecting curves γ_1 and γ_2 resting on the boundary of Ω_w.

The problem in the stated formulation belongs to the class of *mixed boundary value problems with a free boundary* (BVPFB) [5]. Thus, the problem of modeling a horizon surface in the vicinity of tectonic disruptions is reduced to solving a BVPFB in variational formulation.

Remark on solvability. When the functional $E(u)$ is specified as the area functional, the problem reduces to the classical Plateau problem with a free boundary, whose solvability has been studied in [5, 6, 7]. For the case when Γ is a flat polygon, an analytical solution was constructed and its uniqueness was proved by V. N. Monakhov [5]. The formulation (4)–(7) differs by the presence of two cut edges resting on the outer boundary; however, structurally it is close to problems of finding minimal surfaces with a free boundary on manifolds (Schwarz chains [7]), whose solvability has also been established. A complete theoretical study of solvability for an arbitrary form of $E(u)$ is beyond the scope of this work; below, a numerical solution is considered.

3 Algorithm for solving the boundary value problem with the free boundary

3.1 General solution scheme

The numerical solution of the BVPFB is based on an *iterative approach* [8], consisting in repeatedly solving boundary value problems with sequential modification of the unknown part of the boundary at each iteration.

In the original BVPFB, a subproblem is identified in which the condition on the free boundary is absent, and an initial position of the unknown boundary part Γ^0 is chosen. At each iteration $k = 0, 1, 2, \ldots$:

1. **Step 1.** With the fixed position Γ^k, the "truncated" boundary value problem (4)–(6) without condition (7) is solved.

2. **Step 2.** Using the solution obtained in Step 1, the position of the free boundary is corrected so as to reduce the residual of the omitted condition (7).

The condition (7) on the belonging of the cut edges to the fault surface is used as the "omitted" condition. Convergence of the algorithm is considered achieved at the k-th iteration if the Hausdorff distance [9] between two successive approximations of the free boundary Γ^k and Γ^{k+1} satisfies the condition:

$$d_H(\Gamma^k, \Gamma^{k+1}) < \delta \cdot C, \tag{8}$$

where δ is the discretization step of the numerical scheme, and C is an application-dependent constant. In the discrete formulation (see Section 3.2), the Hausdorff distance is replaced by a simpler measure — the maximum vertical deviation of the free boundary points.

The efficiency of the approach depends significantly on the procedure for correcting the free boundary in Step 2. The following sections are devoted to the description of both steps.

3.2 Discretization and numerical solution of the boundary value problem

3.2.1 Justification of the choice of energy functional

The variational principle formulated in Section 2.2 requires specification of the energy functional $E(u)$. Consider two main variants used in geological modeling, and their weighted combination.

Dirichlet energy. Minimization of the functional

$$E_{\mathrm{Lap}}(u) = \int_\Omega |\nabla u|^2 \, dx \, dy \to \min \tag{9}$$

leads to the Laplace equation $\Delta u = 0$ — a linear problem ensuring maximum smoothness. This approach is widely used in existing structural modeling methods [18, 19, 3]. However, in the vicinity of faults, surface gradients can be significant, which makes the purely harmonic approach insufficiently realistic: the surface turns out to be excessively "smoothed," and the fault amplitude is underestimated.

Area functional. A natural nonlinear generalization is the minimization of the area functional

$$E_{\min}(u) = \int_\Omega \sqrt{1 + u_x^2 + u_y^2} \, dx \, dy \to \min, \tag{10}$$

which corresponds to the classical Plateau problem [7]: among surfaces with a given boundary, the one with the smallest area is sought. The Euler–Lagrange equation for the functional (10) is the *minimal surface equation*:

$$\mathcal{L}[u] \equiv \left(1 + u_y^2\right) u_{xx} - 2\, u_x\, u_y\, u_{xy} + \left(1 + u_x^2\right) u_{yy} = 0 \quad \text{in } \Omega. \tag{11}$$

Surfaces satisfying this equation are characterized by zero mean curvature. For small gradients ($|\nabla u| \ll 1$), the nonlinear equation (11) reduces to the linear Laplace equation $\Delta u = 0$, which establishes a direct connection with harmonic interpolation methods.

Minimal surfaces possess properties essential for the problem under consideration: analytical smoothness inside the domain, the maximum principle (absence of local extrema), and minimal deformation relative to the plane. However, using exclusively equation (11) does not allow the geologist to control the surface shape: in some cases, the surface turns out to be too "sharp" in the vicinity of the fault.

Weighted combination. To resolve the contradiction between smoothness and realism, it is proposed to minimize a weighted combination of two functionals:

$$E(u) = \theta\, E_{\mathrm{Lap}}(u) + (1 - \theta)\, E_{\min}(u) \to \min, \tag{12}$$

where $\theta \in [0, 1]$ is a parameter set by the geologist. The Euler–Lagrange equation for the functional (12) is

$$\theta\, \Delta u + (1 - \theta)\, \mathcal{L}[u] = 0 \quad \text{in } \Omega. \tag{13}$$

For $\theta = 1$ this is the Laplace equation, for $\theta = 0$ — the minimal surface equation, and for intermediate values — their combination.

Note that the differential condition (4) in the boundary value problem corresponds to $\theta = 0$ (pure minimal surface); for $\theta > 0$, part of the weight is transferred to the Dirichlet energy, which generalizes the original formulation and gives the geologist additional flexibility.

An important property of the proposed edge-based discretization (Section 3.2.3) is that the discrete analogs of both functionals — E_{Lap} and $E_{\min}$ — are quadratic forms in u. Consequently, their weighted combination is also quadratic, and the minimization problem (12) reduces to solving a single system of linear algebraic equations (SLAE) for any value of θ, despite the fact that the continuous equation (13) is nonlinear for $\theta < 1$. This is a key advantage of the edge-based discretization over the standard finite element method, in which discretization of the area functional leads to a nonlinear system.

The parameter θ is a convenient tool allowing the geologist to control the shape and amplitude of the fault, and has the following geometric meaning (Table 1):

Table 1: Effect of the parameter θ on the surface behavior.

θ	Surface behavior
$\theta = 1$	Pure Laplacian: maximally smooth surface, underestimated fault amplitude
$\theta = 0$	Pure minimal surface: maximum realism, full amplitude
$0 < \theta < 1$	Intermediate regime: the geologist tunes the smoothness/realism balance for a specific fault

3.2.2 Discrete Laplacian

Let T be a triangulation of the domain Ω with edge set $\mathcal{E}$. The discrete analog of the Dirichlet energy is defined as:

$$\Phi_{\text{Lap}}(u) = \sum_{(i,j)\in\mathcal{E}} (u_i - u_j)^2, \tag{14}$$

where u_i, u_j are the values of the sought function at the edge endpoints. Uniform weights are used (the contribution of each edge is the same), which corresponds to the simplest discrete approximation of the Laplace equation on a triangulation. This functional is a quadratic form in u.

3.2.3 Edge-based discretization of the area functional

For the discretization of the area functional (10), an *original edge-based discretization* is proposed, leading to a linear problem.

For each interior edge $e = (i, j)$ separating two triangles with opposite vertices k and l, an auxiliary edge (k, l) is constructed in the xy plane. The edges (i, j) and (k, l) — the diagonals of the quadrilateral formed by the four vertices in the xy plane — intersect at the point p_e (Fig. 3).

Let $t_e \in (0, 1)$ and $s_e \in (0, 1)$ be the parameters determining the position of p_e on the corresponding segments:

$$p_e = (1 - t_e)\, P_i + t_e\, P_j = (1 - s_e)\, P_k + s_e\, P_l, \tag{15}$$

where $P_\cdot$ are the vertex coordinates in the xy plane. The parameters t_e and s_e depend only on the planar geometry of the triangulation and do not depend on the sought function u.

The vertical mismatch of the diagonals at the intersection point:

$$d_e = (1 - t_e)\, u_i + t_e\, u_j - (1 - s_e)\, u_k - s_e\, u_l. \tag{16}$$

The discrete analog of the area functional:

$$\Phi_{\min}(u) = \sum_{e\in\mathcal{E}_{\text{int}}} d_e^2. \tag{17}$$

Asymptotic justification. Expanding u in a Taylor series in the neighborhood of the diagonal intersection point p_e yields

$$d_e = \tfrac{1}{2}\, Q_e(H) + O(h^3),$$

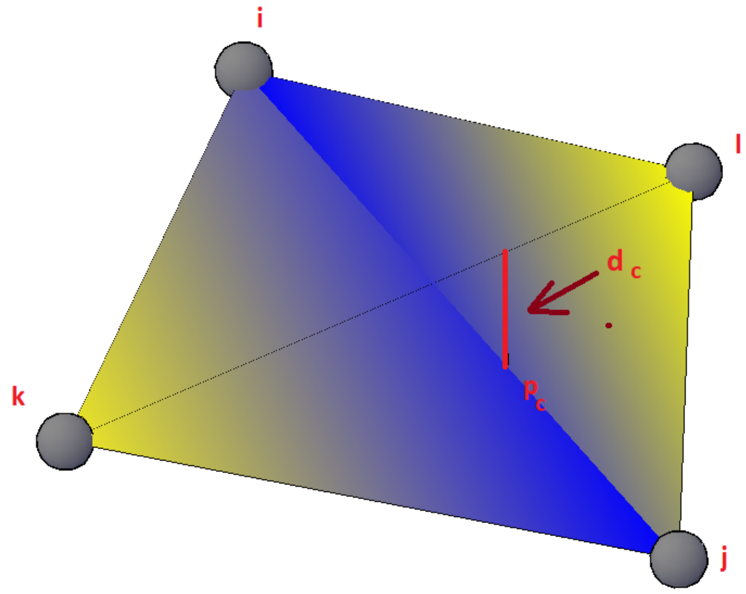

Figure 3: Edge-based discretization. The common edge (i, j) and the auxiliary edge (k, l) are the two diagonals of the quadrilateral formed by a pair of adjacent triangles. The point p_e is the intersection point of the diagonals in the xy plane.

where H is the Hessian matrix of u at p_e, and $Q_e(H)$ is a linear form in its components (u_{xx}, u_{xy}, u_{yy}) depending only on the planar geometry of the quadrilateral. The zeroth- and first-order terms cancel due to the fact that p_e lies on both diagonals. Consequently, $d_e = O(h^2)$, and the functional $\Phi_{\min}$ measures the "bending" of the surface — a quantity determined by second derivatives, as is the minimal surface equation.

The condition $d_e = 0$ means that for the local quadrilateral, the heights along the two diagonals are consistent at their intersection point. For a constant surface, all $d_e = 0$. For surfaces with moderate gradients, condition (17) represents a discrete approximation of the minimal surface equation (11), analogous to the discrete harmonic property: the surface value at the local "center" of the quadrilateral must be consistent in both directions.

The edge-based discretization is related to the result of Rippa [12], in which the values of interpolated functions at the intersection point of the diagonals of a quadrilateral are used to compare the Dirichlet energies of different triangulations. Unlike Rippa's approach, which uses this construction to select an optimal triangulation, in this work it is used directly for surface construction. Compared to the classical cotan formulation of the discrete Laplacian by Pinkall–Polthier [11] and the Laplace–Beltrami operator by Bobenko–Springborn [13], the edge-based discretization provides a simpler geometric interpretation (diagonal consistency) and does not require the computation of trigonometric functions. The study of theoretical properties of the edge-based discretization (maximum principle, convergence rate) is a separate problem.

3.2.4 Weighted combination of discrete functionals

Both functionals (14) and (17) are quadratic forms in u, defined on the same triangulation. Their weighted combination:

$$\Phi(u) = \theta\, \Phi_{\text{Lap}}(u) + (1-\theta)\, \Phi_{\min}(u) \to \min \tag{18}$$

is a quadratic form in u with fixed coefficients (depending only on the planar geometry of the mesh). The minimization of (18) under given boundary conditions is a linear least-squares problem reducible to solving a single SLAE for any value of θ.

3.2.5 Imposition of boundary conditions

Boundary condition of the first kind ($u = h$ on Γ_0). The values of u at the boundary nodes of the triangulation belonging to Γ_0 are fixed and substituted into (14)–(16) as known. The corresponding components of the unknown vector are transferred to the right-hand side of the SLAE.

Boundary condition of the second kind ($\partial u/\partial n = g$ on Γ_0). The technique of *outer boundary extension* is applied. The domain is extended so that not only the boundary nodes belonging to Γ_0 but also the interior nodes adjacent to them (through triangulation edges) fall into the reliable domain. The values of u at these nodes are computed from the given normal derivative g and fixed similarly to the first-kind condition.

Topological condition ($u = w$ on Γ). At the free boundary nodes, the values of u are fixed equal to w. After the next displacement of the free boundary (Section 3.4), these values are recomputed.

3.2.6 Solution of the SLAE

After substituting all fixed values, problem (18) reduces to the linear system

$$A\, \mathbf{u}_{\text{free}} = \mathbf{b}, \tag{19}$$

where $\mathbf{u}_{\text{free}}$ is the vector of unknown values of u at the interior nodes, A is a sparse matrix, and $\mathbf{b}$ is the right-hand side. The matrix A depends on θ and the triangulation geometry but does not depend on the values of u.

The solution is performed by a direct method of sparse LU factorization (SuperLU library [10]).

3.2.7 Iterative scheme

Taking into account the proposed discretization, the k-th iteration of the general algorithm includes:

1. Assembly of the matrix A^k and the right-hand side $\mathbf{b}^k$ for the current triangulation T^k;
2. Solution of the SLAE $A^k\, \mathbf{u}^k = \mathbf{b}^k$ (SuperLU);
3. Construction of the new position of the free boundary Γ^{k+1} (Section 3.4);
4. Retriangulation of T^{k+1} according to the new position of Γ^{k+1} (Section 3.5).

Convergence is monitored by the maximum change in the values of u on the free boundary between successive iterations:

$$\varepsilon^k = \max_{p \in \Gamma^k} \left| u^k(p) - u^{k-1}(p) \right|. \tag{20}$$

The algorithm stops when *stagnation* is reached — when ε^k ceases to decrease:

$$\varepsilon^k \geq \varepsilon^{k-1}. \tag{21}$$

This means that further iterations do not lead to a significant change in the values of u on the free boundary, and the current position Γ^k can be accepted as the sought one.

3.3 Algorithm for constructing the initial triangulation

The main problem in constructing the initial triangulation is determining the initial position of the cut. To solve this problem, the apparatus of combinatorial topology is used [14]. Below we introduce the necessary concepts; details can be found in [14].

Simplicial complex. A finite collection K of simplices (convex hulls of linearly independent sets of points) in the space $\mathbb{R}^m$ is called a simplicial complex if: together with any simplex, the collection contains all its faces; arbitrary simplices intersect properly (along a common face or not at all). The union of all simplices of the complex K is called a *polyhedron* $|K|$.

Connectivity. A polyhedron is called *connected* if for any two of its distinct vertices there exists a path connecting them (a sequence of edges). A homogeneous n-dimensional polyhedron is called *strongly connected* if for any two of its distinct n-dimensional simplices there exists an n-chain connecting them.

Construction of the initial cut

First, a triangulation T_0 is constructed whose boundary is specified by the polyline Γ_0. After that, the variational problem (18) is solved without taking the cut into account. The found function u_0 determines a two-dimensional polyhedron P_u in $\mathbb{R}^3$, whose simplicial scheme is specified by the triangulation T_0. Similarly, it is assumed that the fault surface function w determines a polyhedron P_w.

The intersection of the polyhedra is taken as the initial position of the cut:

$$P_\gamma = P_u \cap P_w. \tag{22}$$

It is assumed that P_γ is a spatial polyline without self-intersections, whose ends rest on the boundary of the polyhedron P_u, and whose projection onto the xy plane is a planar polyline without self-intersections, whose ends rest on the boundary of Ω. In practice, these conditions are ensured manually — either by extending the boundary of the unreliability domain (modifying the shape of P_u) or by editing the fault surface (modifying the shape of P_w).

To construct the initial triangulation T^0, it is proposed to first construct an intermediate *constrained triangulation* T_c [15] containing the vertices and edges of the polyline P_γ, and then perform a *topological cut* along the specified edges.

3.4 Algorithm for constructing the new position of the free boundary

3.4.1 Displacement of interior points

The traditional technique for moving the free boundary is based on specifying the velocity of points along the normal vector to the curve defining the boundary [16]. This approach requires boundary smoothness. For the free boundary in the problem under consideration, only one-sided normals exist along each of the cut edges γ_1 and γ_2, and at the cut vertices A and B, two-sided normals do not exist. Moreover, the cut vertices are subject to an additional constraint — they must belong to the boundary Γ_0.

Thus, the traditional technique is applicable only to the interior points of the curves γ_1 and γ_2, while for the vertices A and B special displacement mechanisms are needed. Using different displacement methods within a single algorithm would lead to boundary inconsistency. To solve this problem, an *algebraic approach* is proposed, combining the traditional technique with a mechanism for smooth boundary transformation.

Let p be an interior point of the cut edge γ_i. The new position is specified by the expression

$$p' = p + \lambda\,\mathbf{n}, \tag{23}$$

where $\mathbf{n}$ is the unit normal to the reference curve at the point p, and λ is the displacement magnitude. The value of λ is chosen from the condition of satisfying the omitted condition (7). Taking into account that for minimal surfaces the derivative along the normal to the free boundary is zero, and using a first-order approximation of the function w through its derivative, we obtain:

$$\lambda \approx \frac{w(p) - u(p)}{\nabla w \cdot \mathbf{n}}. \tag{24}$$

Essentially, λ determines the length of the projection vector of the three-dimensional point p onto the fault surface specified by the function w, along the normal vector $\mathbf{n}$.

Uniqueness of the intersection is guaranteed for a plane and surfaces with small curvature. As the edge of the free boundary approaches the minimum, maximum, or saddle points of the fault surface, the probability of intersection uniqueness decreases. In practice, such problems are resolved at the stage of editing fault surfaces — by smoothing or splitting complex surfaces.

3.4.2 Displacement of cut vertices

Let A^k and B^k be the positions of the cut vertices at the k-th iteration. By definition, both vertices belong to Ω_w; however, in general, the three-dimensional points $u(A^k)$ and $u(B^k)$ do not lie on the fault surface, i.e., $u(A^k) \neq w(A^k)$ and $u(B^k) \neq w(B^k)$.

It is assumed that the surface w is *monotone* along the boundary of Ω_w at the locations where the cut vertices move: as the point moves along the boundary, the value of w monotonically increases or decreases. To satisfy condition (7), the vertices are displaced along the boundary until the values $w(A)$ and $w(B)$ are reached, respectively:

$$u(A^{k+1}) = w(A^{k+1}), \qquad u(B^{k+1}) = w(B^{k+1}). \tag{25}$$

The resulting displacement vectors are called *projective boundary vectors* and are denoted $\mathbf{b}_1$ (for vertex A) and $\mathbf{b}_2$ (for vertex B).

3.4.3 Consistent boundary transformation

Using different displacement methods for interior and boundary points leads to boundary inconsistency in the vicinity of the cut vertices, since the projective boundary vectors $\mathbf{b}_1$, $\mathbf{b}_2$ and the projective normal vectors (23)–(24) are not consistent with each other.

To construct a consistent transformation, it is proposed to construct the projective vector at each interior point p of the edge γ_i as a *weighted sum* of the normal to the curve and the projective boundary vectors.

Let $t \in [0, 1]$ be the parameter of the point p under the parametrization of the curve γ_i (directed from vertex A to vertex B). The new projective vector:

$$\mathbf{v}(t) = (1 - \alpha_1(t) - \alpha_2(t))\,\mathbf{n}(t) + \alpha_1(t)\,\mathbf{b}_1 + \alpha_2(t)\,\mathbf{b}_2, \tag{26}$$

where $\mathbf{n}(t)$ is the normal to the curve at the point $p(t)$, $\mathbf{b}_1$ and $\mathbf{b}_2$ are the projective boundary vectors for vertices A and B, respectively, and $\alpha_1(t)$ and $\alpha_2(t)$ are weight functions satisfying the conditions:

1. $0 \leq \alpha_1(t),\, \alpha_2(t) \leq 1$ for all $t \in [0, 1]$;
2. $\alpha_1(0) = 1$, $\alpha_2(1) = 1$ (at the ends of the edge, the projective vector coincides with the corresponding boundary vector);
3. $\alpha_1(1) = 0$, $\alpha_2(0) = 0$;
4. $\alpha_1(t)$, $\alpha_2(t) \to 0$ when moving away from the corresponding end of the segment.

The following weight functions (second-order polynomials) are chosen:

$$\alpha_1(t) = (1 - t)^2, \qquad \alpha_2(t) = t^2. \tag{27}$$

In this case, at the endpoints of the edge, the projective vector equals the corresponding projective boundary vector, and at the midpoint ($t = 0.5$) — the normal to the curve. The behavior of the projective vector is continuous, and its smoothness is determined by the smoothness of the weight functions. Practice shows that second-order polynomials are sufficient for stable boundary behavior and acceptable convergence of the numerical algorithm.

The new position of the interior point $p(t)$ is determined as

$$p'(t) = p(t) + \mathbf{v}(t). \tag{28}$$

3.5 Retriangulation

After obtaining the new position of the free boundary Γ^{k+1}, the triangulation is reconstructed. In the standard case (cut edges do not intersect), the reconstruction is performed by Delaunay triangulation algorithms with constraints [15], provided that the topology of the cut is preserved (preservation of the number of components and the orientation of the vertex traversal of triangles).

For significant displacements of nodes, the correctness of the triangulation may be violated (change of vertex traversal orientation, overlapping of triangles). In this case, reconstruction based on the “bubble meshing” technique [17] is applied, in which the

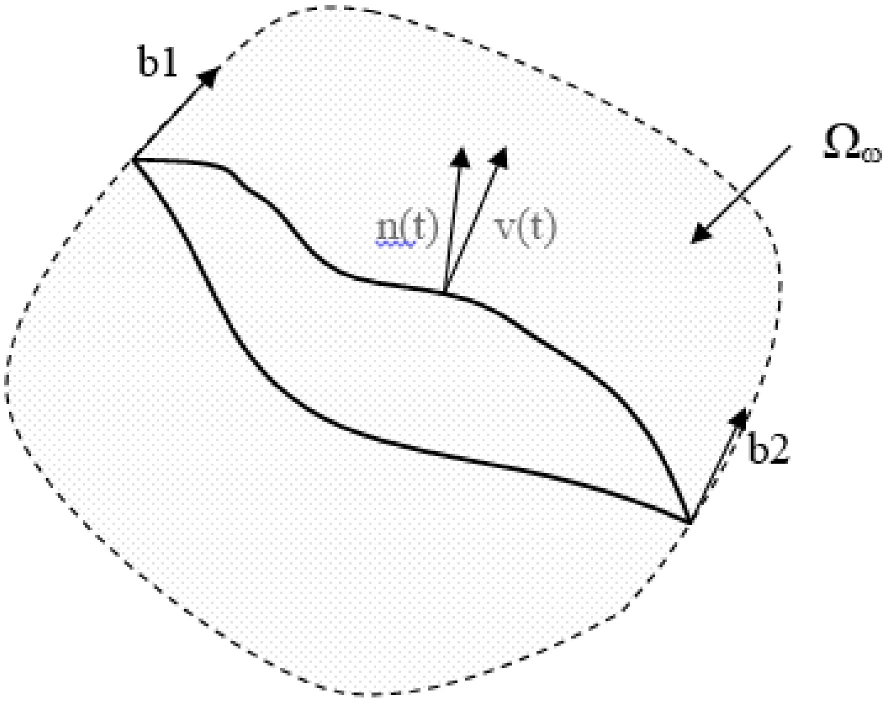

Figure 4: Consistent boundary transformation. At each interior point of the cut edge, the projective vector $\mathbf{v}(t)$ is constructed as a weighted sum of the normal $\mathbf{n}(t)$ and the projective boundary vectors $\mathbf{b}_1$, $\mathbf{b}_2$.

triangulation nodes are considered as centers of virtual "bubbles" of a given diameter, and their positions are adjusted under the action of repulsive forces between neighboring nodes. A mixed strategy — using standard reconstruction until a threshold displacement is reached and switching to "bubble meshing" when it is exceeded — ensures robustness at moderate computational cost.

4 Handling self-intersection of cut edges

The algorithm described above assumes that during iterations, the cut edges γ_1 and γ_2 do not intersect, and the domain Ω remains doubly connected with a simple (non-self-intersecting) inner boundary Γ. In practice, however, for certain fault geometries, the cut edges may intersect in projection onto the xy plane. The formal statement of the boundary value problem (4)–(7) ceases to be directly applicable in this case, since the domain Ω is no longer doubly connected with a simple boundary.

Below, a practical approach to handling this situation is described, based on decomposing the domain into subdomains with simple boundaries. A complete formalization within the framework of cellular atlas theory will be presented in a separate publication.

4.1 Geometric interpretation of self-intersection

The self-intersection of the cut edges γ_1 and γ_2 in projection onto the xy plane means that the horizon surface ceases to be uniquely representable by a single function $u(x, y)$ on the entire domain Ω: in the intersection zone, the edges of the horizon overlie each other.

Geometrically, this corresponds to the transition from a normal fault to a reverse fault (thrust) on the horizon surface. The surface remains locally representable as a function at every point, but globally requires decomposition into several functional charts — one for each subdomain where the representation remains unique.

4.2 Detection of self-intersection

Self-intersection of the edges is detected indirectly — through the incorrectness of the reconstructed triangulation. After displacing the free boundary nodes and reconstructing the triangulation, the orientation of the vertex traversal of all triangles is checked. Violation of the orientation or overlapping of triangles indicates that the contour $\Gamma = \gamma_1 \cup \gamma_2$ has ceased to be a simple curve.

4.3 Domain decomposition

Upon detection of self-intersection, it is proposed to decompose the domain Ω into two simply connected subdomains by making two additional cuts:

1. a cut from vertex A to the nearest point on the outer boundary Γ_0, passing inside Ω;
2. a cut from vertex B to the nearest point on the outer boundary Γ_0, passing inside Ω.

Each cut is the shortest path from the corresponding vertex to the outer boundary through the interior of the domain. As a result, the original domain Ω is decomposed into two subdomains Ω_1 and Ω_2 (Fig. 5). Each subdomain is simply connected with a simple boundary and contains its own portion of the cut boundary.

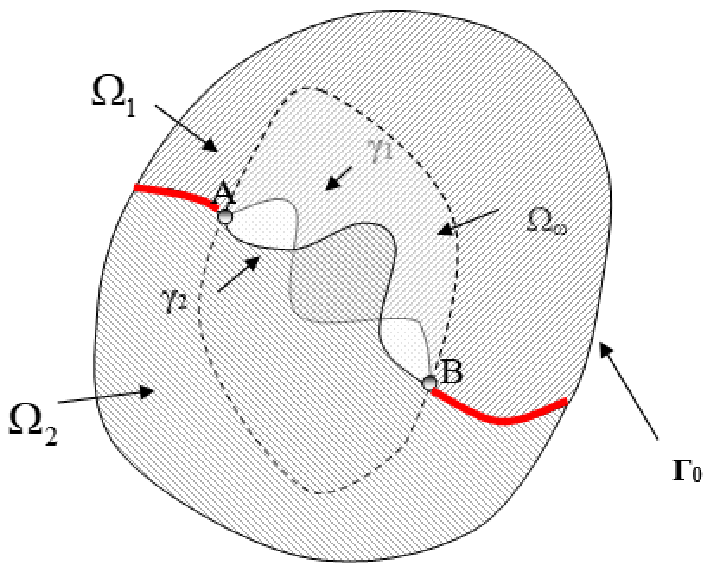

Figure 5: Domain decomposition upon self-intersection of cut edges. Edges γ_1 and γ_2 have intersected. Vertices A and B on the boundary of Ω_w. Two cuts from A and B to the nearest points on Γ_0. The domain Ω is decomposed into two simply connected subdomains Ω_1 and Ω_2.

4.4 Triangulation and stitching

Since the boundary of each subdomain Ω_i is a simple closed curve, standard constrained Delaunay triangulation algorithms [15] are applicable to each subdomain separately. Let the resulting triangulations be T_1 and T_2.

The stitching of triangulations T_1 and T_2 along the cuts is performed by identifying pairs of nodes on the common edges of the cuts. This operation is the reverse of the topological cut: instead of separating vertices on the cut, their merging is performed. The result is a single triangulation T^{k+1} whose topological structure is correct, even if the geometric embedding of individual triangles in the xy plane contains overlaps.

4.5 Solving the SLAE on the stitched triangulation

The key property of the edge-based discretization (Section 3.2.3) is that the SLAE matrix A is constructed solely on the basis of the topological adjacency of triangles and the parameters t_e, s_e computed from the planar geometry of the edges. The parameters t_e, s_e are computed before solving the SLAE and are fixed at the current iteration. Consequently, the assembly and solution of the linear system (19) on the stitched triangulation proceeds without regard to the fact that the geometric embedding of some triangles may be incorrect. The topological structure of the stitched triangulation completely determines the matrix A^k, and the solution of the system yields a correct approximation to the minimal surface on each of the subdomains.

This property significantly distinguishes the proposed edge-based approach from traditional finite element methods, in which the stiffness matrix depends on the geometric characteristics of the elements and requires geometric correctness of the triangulation.

4.6 Connection with reverse faults

The described decomposition of the domain into two simply connected subdomains naturally corresponds to the geometry of a reverse fault (thrust). Upon self-intersection of the edges, the horizon surface in the thrust zone is represented not by a single function but by two — one for each subdomain. The set of these functional representations forms the simplest atlas of two functional charts, analogous to the Osserman construction for minimal surfaces [7].

Further generalization — to the case of multiple faults, intersecting faults, and complex fault networks — requires the development of a complete theory of cellular CW-atlases and will be considered in a separate publication. This section demonstrates that the proposed algorithm naturally generalizes from a normal fault to a reverse fault without changing the computational scheme: the only requirement is correct reconstruction of the triangulation through decomposition into subdomains and stitching.

5 Model tests

Obviously, the algorithm formulated above cannot provide a solution for an arbitrary set of input data. However, our goal is to obtain a practical algorithm, i.e., to guarantee that a solution is obtained for input data corresponding to real geological objects. For this purpose, a set of tests is proposed. The main goal of testing is to verify the practical applicability of the algorithm. On the other hand, it is necessary to investigate the influence of fault and horizon geometry on the stability and convergence rate of the developed algorithm. This is needed to organize "feedback," i.e., requirements for input data that can be satisfied at the preprocessing stage.

The following set of measures is proposed for investigating the convergence of tests:

- average displacement length of free boundary points ($\bar{d}$);
- maximum displacement length of free boundary points ($d_{\max}$);
- average vertical deviation of modeled surface points ($\bar{\varepsilon}$);
- maximum vertical deviation of free boundary points ($\varepsilon_{\max}$).

5.1 Setup of model tests

In model testing, the case of a single fault is considered. The unreliability domain is a square with side 100 m. The unreliability domain is adjacent to the reliable domain along three sides; the fourth side is free. To the left of the symmetry axis, the horizon surface has value 0, to the right — $h = 50$ m. The fault surface is a half-plane raised to height $h/2$ and rotated by angle α (Fig. 6). The quantity h specifies the fault amplitude, and the angle α specifies the inclination angle of the projection plane.

The stagnation criterion (Section 3.2.7) is used as the stopping criterion: the algorithm stops when the maximum vertical deviation of the free boundary points ε^k ceases to decrease ($\varepsilon^k \geq \varepsilon^{k-1}$). Additionally, the achieved accuracy — the ratio of ε^k to the fault amplitude h — is recorded.

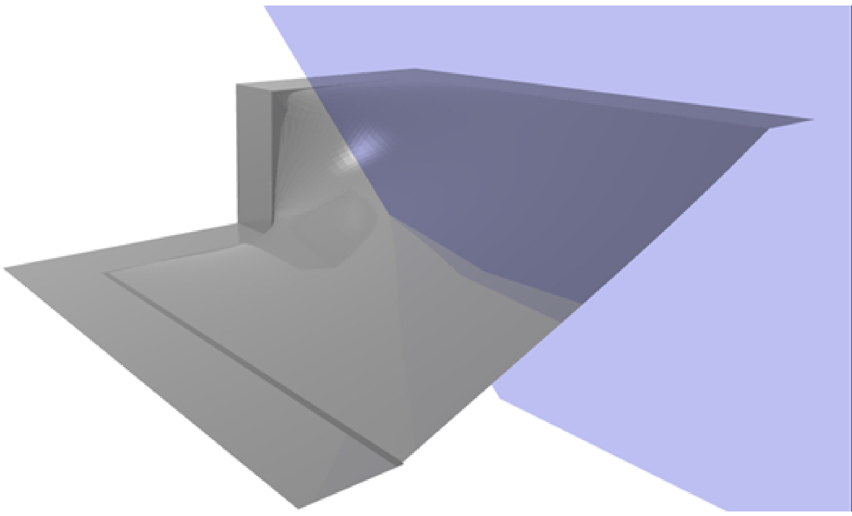

Figure 6: Model test: unreliability domain (square), primary horizon surface (step function), and fault plane (half-plane rotated by angle $\alpha = 135°$).

5.2 Effect of the parameter θ

Tests were conducted at a fixed $\alpha = 45°$ for three values of the parameter $\theta = 0.3$; 0.5; 0.7 (Table 2).

Table 2: Effect of the parameter θ at $\alpha = 45°$, $h = 50$ m, normal fault.

θ	Iter.	$\bar{d}$ (m)	d_{max} (m)	ε_{max} (m)
0.3	11	0.0291	0.0632	0.0722
0.5	8	0.0251	0.0516	0.0601
0.7	6	0.0175	0.0327	0.0335

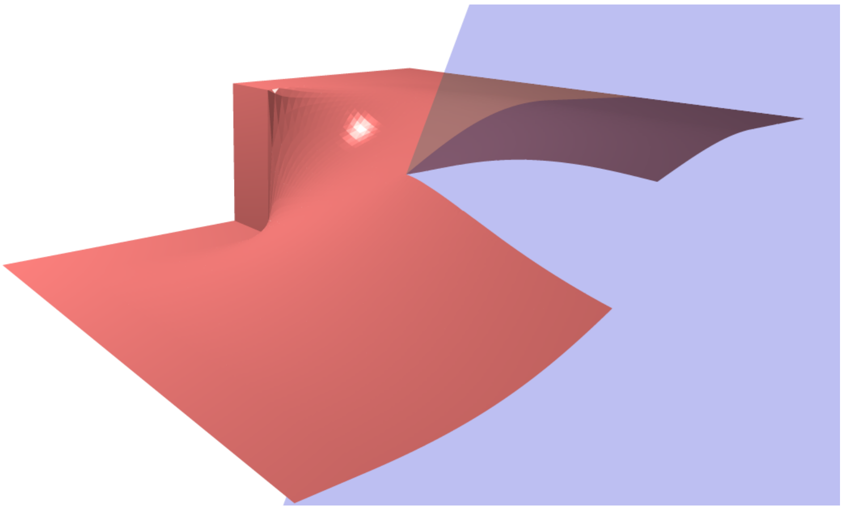

Figure 7: Resulting horizon surfaces for $\theta = 0.5$ and $\alpha = 45°$.

The parameter θ has a significant effect on the surface shape: for $\theta = 0.7$ (Laplacian predominance), the surface is smoother and the fault amplitude is underestimated; for $\theta = 0.3$ (minimal surface predominance), the surface more closely follows the fault geometry but requires more iterations. The value $\theta = 0.5$ provides an acceptable balance.

5.3 Effect of the inclination angle α

The dependence of the convergence rate on the angle α was investigated at a fixed $\theta = 0.5$. Both a normal (direct) fault ($\alpha = 45°; 60°$) and a reverse fault — thrust ($\alpha = 120°; 135°; 150°$) — were considered. The results are presented in Table 3.

Table 3: Effect of the angle α at $\theta = 0.5$, $h = 50$ m. Three convergence measures at the last iteration.

α (°)	Type	Iter.	$\bar{d}$ (m)	d_{max} (m)	ε_{max} (m)
45	normal	8	0.0251	0.0516	0.0601
60	normal	7	0.0237	0.0467	0.0501
120	reverse	11	0.0197	0.0373	0.0456
135	reverse	5	0.0131	0.0173	0.0265
150	reverse	12	0.0372	0.0393	0.0745

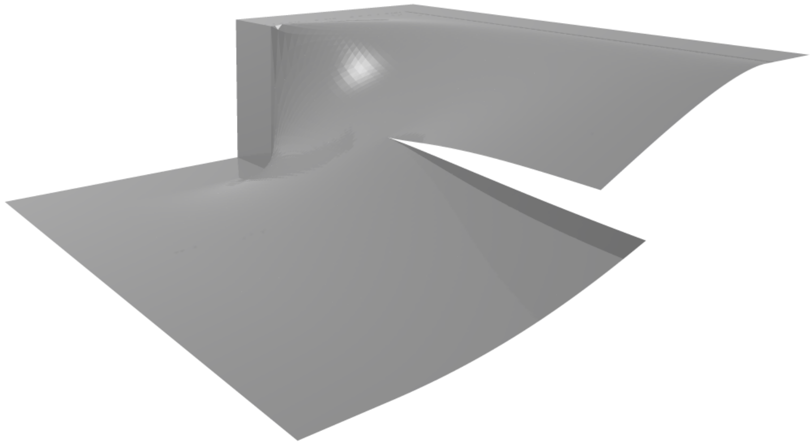

Figure 8: Resulting horizon surface for a reverse fault ($\alpha = 135°$).

5.4 Non-planar (spherical) fault

Experiments were conducted with a non-planar fault, where a segment of a sphere was used as the fault surface. The influence of curvature (radius) on the convergence rate was investigated (Table 4).

Table 4: Non-planar (spherical) fault at $\theta = 0.5$, $h = 50$ m. R is the sphere radius.

R (m)	Iter.	$\bar{d}$ (m)	$d_{\max}$ (m)	$\varepsilon_{\max}$ (m)
1000	12	0.0173	0.0311	0.0471
500	14	0.0182	0.0345	0.0485
300	17	0.0213	0.0401	0.0541

5.5 Analysis of model test results

Analysis of the results of experiments on test models shows that for the working range of angles ($\alpha > 30°$) of the projection plane inclination, a few iterations are sufficient to achieve acceptable accuracy (hundredths of the fault amplitude). Faults with inclination angles less than 30° require special handling. At small angles, the accuracy of the procedure for projecting free boundary points onto the fault surface deteriorates, and the displacement of mesh nodes during triangulation reconstruction increases.

All four investigated measures behave in the same way; therefore, any of them can be used for convergence control. The least computational effort is required by the "maximum vertical deviation of free boundary points" ($\varepsilon_{\max}$), which is used for testing the algorithm on real geological models.

For a spherical fault, the influence of curvature on the convergence rate is insignificant for surfaces with a radius of curvature substantially exceeding the fault amplitude. As the radius of curvature decreases (presence of minimum, maximum, or saddle points), the probability of projection uniqueness decreases, which requires additional preprocessing of the fault surface.

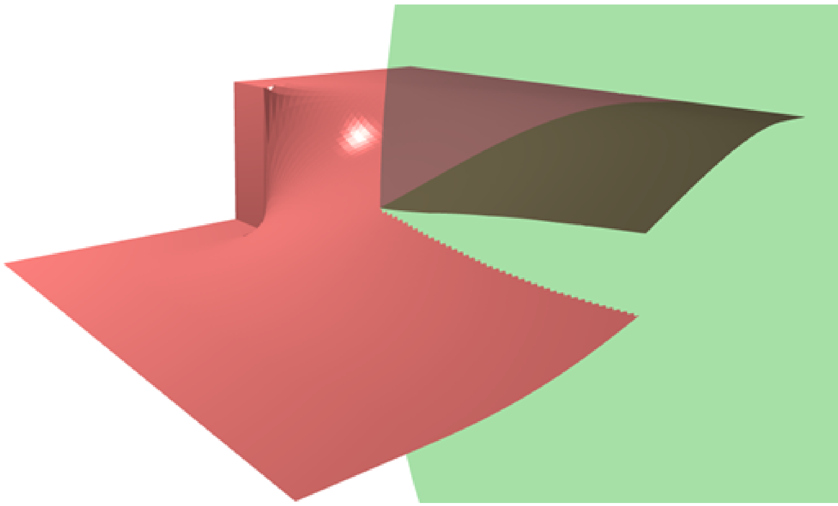

Figure 9: Resulting horizon surface for a spherical fault (sphere segment).

6 Testing on real geological objects

The set of tests on real geological objects was selected based on the criterion of maximum representativeness. Objects were selected that would differ significantly from each other and maximally cover the range of real geological situations. For formalization, the following characteristics of the structural model were chosen: grid step for constructing the primary horizon surface; number of faults; average and minimum inclination angles of fault projection planes (Table 5).

Table 5: Characteristics of real geological models.

Model	Grid step (m)	Number of faults	Min. angle (°)	Avg. angle (°)
Krasnoslobodsky fault Starobinskoye deposit	500.0	7	33.0	44.0
Central tectonic fault Starobinskoye deposit	200.0	9	35.0	41.0
Deep-water fault “Neptun”	100.0	15	22.0	37.4
Fault zone TWAKE	50.0	8	27.1	35.7

Testing on real objects was primarily intended to assess the robustness of the algorithm to the real geometry of stratiform deposits under intensive tectonic disruptions. The maximum vertical deviation of free boundary points at each step, normalized by the minimum average distance between strata, was used as the convergence criterion. The algorithm stopped when this quantity became less than one hundredth of the average distance between strata.

During testing, neighborhoods of the intersection of the fault system with the primary horizon surface were used as the initial unreliability domains. The neighborhood radius was chosen equal to twice the diagonal of the grid cell on which the primary horizon surface is defined. If the initial conditions of the algorithm were not satisfied, the neighborhood radius was manually adjusted to enable the algorithm to start.

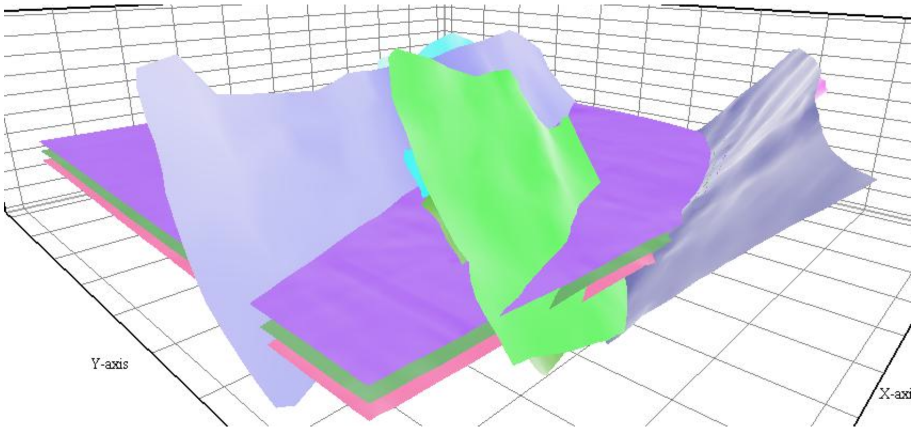

Figure 10: Initial horizon and fault surfaces of the TWAKE model.

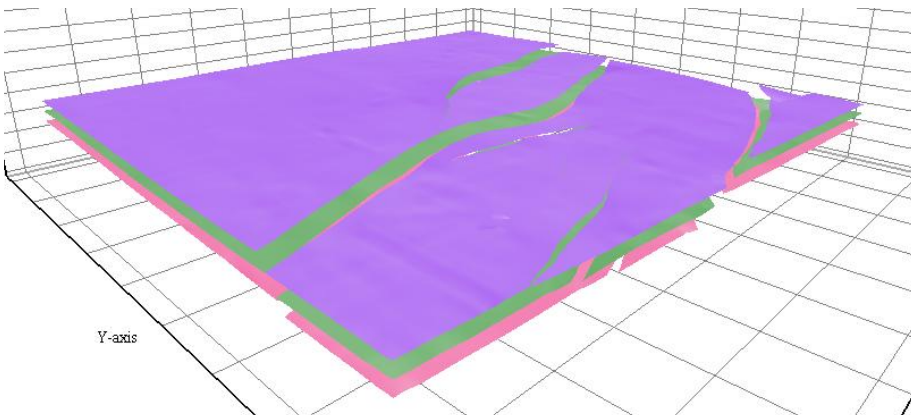

Figure 11: Resulting horizon surfaces of the TWAKE model obtained by the algorithm.

Table 6: Results of testing on real geological models: average and maximum number of iterations, average displacement length of free boundary points, average vertical deviation of modeled surface points.

Model	Avg. iter.	Max. iter.	$\bar{d}$ (m)	$\bar{\varepsilon}$ (m)
Krasnoslobodsky fault	10	15	0.06	0.07
Central tectonic fault	9	15	0.03	0.05
Deep-water fault “Neptun”	14	17	0.06	0.07
Fault zone TWAKE	11	16	0.05	0.07

Analysis of the results on real geological models shows that the algorithm is quite sensitive to the value of the minimum inclination angle of fault projection planes. Faults with small angles lead to an increase in the required number of iterations and often can lead to incorrect termination of the algorithm. This is related not only to the deterioration of the accuracy of the procedure for projecting free boundary points onto the fault surface at small angles but also to significant displacement of mesh nodes during triangulation reconstruction.

In conclusion of the discussion of the problem of faults with small inclination angles, we note that they are rather specific objects in structural geology and have a special designation "thrust fault" in English terminology. Due to their significant horizontal extent, they are generally considered as surfaces of additional horizons in structural modeling.

7 Discussion

The proposed approach has two key differences from existing structural modeling methods. First, unlike implicit methods [1, 2, 18], in which the intersection of the horizon with the fault is determined a posteriori, the proposed formulation specifies the cut as part of the boundary value problem — a free boundary whose position is determined together with the surface. This ensures topological correctness by construction. Second, unlike the standard finite element discretization of the area functional, which leads to a nonlinear system (the stiffness matrix depends on the solution), the proposed edge-based discretization yields a quadratic form with fixed coefficients. As a result, each step of the iterative process reduces to solving a single linear system, regardless of the value of θ.

The parameter θ is a practical modeling tool. Decreasing θ brings the surface closer to a minimal surface — the fault amplitude increases and the shape becomes more realistic. Increasing θ shifts the balance toward Laplacian interpolation — the surface is smoothed and the amplitude decreases. If the constructed surface appears excessively "sharp" near the fault, θ is increased; if the fault amplitude appears underestimated, θ is decreased. The value $\theta = 0.5$ is recommended as an initial approximation, providing a balanced regime for typical fault geometries.

The limitations of the algorithm are primarily related to the geometry of the fault surface. For inclination angles of the projection plane below 30°, the accuracy of the procedure for projecting free boundary points onto the fault surface deteriorates, and the displacement of mesh nodes during triangulation reconstruction increases, which can lead to unstable behavior of the algorithm. Faults with small inclination angles (thrust faults) have significant horizontal extent and are generally treated as surfaces of additional horizons in structural modeling practice. Uniqueness of projection is guaranteed for planar fault surfaces and surfaces with small curvature; in the presence of extrema (minima, maxima, saddles) on the fault surface, preliminary smoothing or partitioning of the complex surface into segments is required.

8 Conclusion

The article proposes a mathematically justified approach to constructing a geological horizon surface in the vicinity of a single tectonic fault. The problem of recovering the unreliable part of the surface is reduced to a mixed boundary value problem with a free boundary in a variational formulation, in which the sought surface is defined as a minimizer of an energy functional.

An original edge-based discretization of the area functional is developed, and a weighted combination of the Dirichlet energy and the area functional controlled by the parameter θ is proposed. For $\theta = 1$, the approach coincides with known harmonic interpolation methods; for $\theta = 0$ — with minimal surfaces; intermediate values give the geologist a flexible tool for tuning the surface shape for specific fault characteristics. The proposed formulation is *linear by construction* for any θ — the coefficients depend only on the planar mesh geometry and do not depend on the solution. This ensures computational efficiency (one SLAE per iteration, solved by direct sparse LU factorization) and robustness.

A practical approach to handling self-intersection of cut edges is described, naturally extending the algorithm to the case of reverse faults. The key property ensuring the algorithm's operability under self-intersection is the topological nature of the edge-based discretization: the SLAE matrix depends only on the adjacency structure of triangles and not on their geometric embedding.

The results of model tests confirm the practical applicability of the algorithm and show that the parameter θ allows effective control of the balance between surface smoothness and realism. Testing on real geological models — the Krasnoslobodsky fault, the central tectonic fault of the Starobinskoye deposit, the deep-water fault "Neptun," and the fault zone TWAKE — demonstrated the robustness of the algorithm under intensive tectonic disruptions. The algorithm successfully completes operation when the minimum inclination angle of fault projection planes exceeds 30°; for smaller angles, special handling is required due to the deterioration of the accuracy of the procedure for projecting free boundary points onto the fault surface and the increase in mesh node displacement during triangulation reconstruction. Faults with small inclination angles (thrust faults) have significant horizontal extent and are generally considered as surfaces of additional horizons in structural modeling.

Generalization of the proposed approach to the case of systems of arbitrary faults (including thrusts and fault networks) will be considered in a separate publication.

References

[1] Lajaunie C., Courrioux G., Manuel L. Foliation fields and 3D cartography in geology: principles of a method based on potential interpolation // Mathematical Geology. — 1997. — Vol. 29, No. 4. — P. 571–604.

[2] Calcagno P., Chilès J. P., Courrioux G., Guillen A. Geological modelling from field data and prior knowledge // Physics of the Earth and Planetary Interiors. — 2008. — Vol. 171, No. 1–4. — P. 158–169.

[3] Mallet J.-L. Discrete smooth interpolation // ACM Transactions on Graphics. — 1989. — Vol. 8, No. 2. — P. 121–144.

[4] Hu L. G. Gradual deformation and Kalman filter // Mathematical Geosciences. — 2009. — Vol. 41. — P. 311–326.

[5] Monakhov V. N. Boundary value problems with free boundaries for elliptic systems of equations. — Novosibirsk: Nauka, 1977. (In Russian)

[6] Friedman A. Variational Principles and Free-Boundary Problems. — New York: Wiley, 1982.

[7] Courant R. Dirichlet's Principle, Conformal Mapping, and Minimal Surfaces. — New York: Interscience, 1950.

[8] Crank J. Free and Moving Boundary Problems. — Oxford: Clarendon Press, 1987.

[9] Hausdorff F. Grundzüge der Mengenlehre. — Leipzig: Veit, 1914.

[10] Demmel J. W., Eisenstat S. C., Gilbert J. R., Li X. S., Liu J. W. H. A supernodal approach to sparse partial pivoting // SIAM Journal on Matrix Analysis and Applications. — 1999. — Vol. 20, No. 3. — P. 720–755.

[11] Pinkall U., Polthier K. Computing discrete minimal surfaces and their conjugates // Experimental Mathematics. — 1993. — Vol. 2, No. 1. — P. 15–36.

[12] Rippa S. Minimal roughness property of the Delaunay triangulation // Computer Aided Geometric Design. — 1990. — Vol. 7. — P. 489–497.

[13] Bobenko A. I., Springborn B. A. A discrete Laplace–Beltrami operator for simplicial surfaces // Discrete & Computational Geometry. — 2007. — Vol. 38, No. 4. — P. 740–756.

[14] Yakovlev E. I. Introduction to combinatorial topology. — Nizhny Novgorod: Nizhny Novgorod State University Press, 2004. (In Russian)

[15] Shewchuk J. R. Triangle: Engineering a 2D Quality Mesh Generator and Delaunay Triangulator // Applied Computational Geometry: Towards Geometric Engineering. — LNCS 1148, 1996. — P. 203–222.

[16] Sethian J. A. Level Set Methods and Fast Marching Methods. — Cambridge: Cambridge University Press, 1999.

[17] Shimada K., Gossard D. C. Bubble mesh: automated triangular meshing of non-manifold geometry by sphere packing // Proceedings of the 3rd Symposium on Solid Modeling and Applications. — 1995. — P. 409–419.

[18] Irakarama M., Laurent G., Renaudeau J., Caumon G. Finite difference implicit modeling of geological structures // Mathematical Geosciences. — 2020. — Vol. 53. — P. 785–808.

[19] Renaudeau J., Malvesin E., Maerten F., Caumon G. Implicit structural modeling by minimization of the bending energy with moving least squares functions // Mathematical Geosciences. — 2019. — Vol. 51. — P. 693–724.

[20] Mallet J.-L. Geomodeling. — Oxford: Oxford University Press, 2002.

[21] Frank T., Tertois A.-L., Mallet J.-L. 3D-reconstruction of complex geological interfaces from non-regularly spaced data // Computers & Geosciences. — 2007. — Vol. 33, No. 7. — P. 932–943.

[22] Caumon G., Collon-Drouaillet P., Le Carlier de Veslud C., Sausse J. Surface-based 3D modeling of geological structures // Mathematical Geosciences. — 2009. — Vol. 41, No. 8. — P. 927–945.

[23] Sprague K. B., de Kemp E. A. Implication of approximating stratigraphic surfaces: a case study from western Canada // Geosphere. — 2006. — Vol. 2, No. 6. — P. 340–352.

[24] Laurent G., Caumon G., Bouziat A. A parametric method to model 3D faults and fault networks // Mathematical Geosciences. — 2013. — Vol. 45. — P. 759–775.